Prepared for submission to JCAP

Primordial features and low-ℓ suppression from isocurvature modes in multi-field Higgs–R^2 inflation

Flavio Pineda [a,1] **Luis O. Pimentel** [a,2]

[a]Departamento de Física, Universidad Autónoma Metropolitana Iztapalapa P. O. Box 55-534, 09340 México, CDMX., México

E-mail: fpineda@xanum.uam.mx, lopr@xanum.uam.mx

Abstract. We study primordial perturbations in Higgs–R^2 inflation in the presence of a non-minimal kinetic mixing between the Higgs and the scalaron. By performing a full numerical integration of the multifield background and linear perturbations, we identify distinct dynamical regimes controlled by the non-minimal coupling ξ_h. For $\xi_h \sim \mathcal{O}(0.1)$, the turning rate of the inflationary trajectory induces transient multifield effects that imprint localized features in the scalar power spectrum. In the limit $\xi_h \ll 1$, the adiabatic spectrum becomes featureless, but isocurvature modes fail to fully decay, leaving a residual contribution at the end of inflation. We compute CMB angular power spectra TT, TE, EE and show how these regimes yield distinct observational signatures, delineating the parameter space compatible with current bounds. Our results highlight that suppressing spectral features does not guarantee the elimination of isocurvature perturbations, placing non-trivial constraints on Higgs–R^2 multifield realizations and motivating future probes sensitive to primordial isocurvature.

Contents

1 Introduction

Cosmic inflation has become the leading paradigm of early-universe cosmology, providing a natural explanation for the horizon problem and the origin of the primordial perturbations imprinted in the Cosmic Microwave Background (CMB) [1–3]. In its simplest realization, inflation is driven by a single scalar field and predicts a nearly adiabatic and scale-invariant spectrum [4], in excellent agreement with Planck observations [5]. However, realistic high-energy theories, such as supersymmetry, Grand Unified Theories (GUTs), or string theory contain multiple scalar degrees of freedom. Multi-field inflation therefore arises naturally [6], allowing for isocurvature modes, non-trivial field-space geometries, and turning trajectories that can impact the primordial power spectrum [7–14]. These features may produce observable signatures, including localized departures from scale invariance or correlated isocurvature contributions and primordial non-Gaussianity [15–21]. Well-studied examples include models with non-minimal couplings [22–24], kinetic mixing [9, 25, 26], and scenarios involving heavy fields [27–29]. Within this broad context, the Higgs-R^2 model stands out as a theoretically appealing multi-field inflation [30–33]. It links cosmic inflation to the Standard Model (SM) Higgs boson while simultaneously resolving the unitarity problem of Higgs inflation [30, 34–36]. The addition of a curvature-squared term introduces an extra scalar degree of freedom and raises the cutoff scale to the Planck scale, thereby restoring perturbative control [36]. Even though the model is often treated in an effective single-field limit [31, 32], its true dynamics are intrinsically multi-field, governed by a curved field-space metric that mixes the Higgs and the scalaron.

The Higgs-R^2 model has been explored in a wide range of contexts, including preheating [37–40], gravitational particle production and primordial magnetogenesis [41, 42], cosmological collider signatures [43], gravitational waves [44], primordial black-hole formation [45, 46] and more recently in relation to small-scale CMB experiments [47]. In this work, we revisit the multi-field dynamics of Higgs-R^2 inflation, focusing on the region of parameter space where the single-field attractor description ceases to be valid. In particular, we study the regime where the non-minimal Higgs coupling is small, $\xi_h \sim 0.1$, such that no strong hierarchy between the fields exists. In this case, the inflationary trajectory may deviate from the valley and undergo transient turns as it evolves from the ridge at $h = 0$ toward the minima [33]. These turns generate a non-zero bending rate $\eta_\perp$, which couples adiabatic and isocurvature perturbations and can leave distinctive signatures in the primordial spectrum, such as features or a suppression of power at large scales. Despite the growing interest in this model, the literature still lacks a systematic analysis of the simultaneous evolution of adiabatic and isocurvature modes, the role of transient turning trajectories, the emergence of features in $\mathcal{P}_\mathcal{R}(k)$, and their observable imprint on the CMB angular spectra.

Our motivation is twofold. From a theoretical perspective, understanding the robustness of inflationary predictions when isocurvature modes are not suppressed is essential for assessing the predictivity of multi-field models. Observationally, the Planck 2018 data [5] reveals intriguing anomalies at large angular scales, most notably a suppression of power in the quadrupole ($\ell = 2$) and octupole ($\ell = 3$) moments. While standard ΛCDM attributes this to cosmic variance, physical mechanisms producing localized features in the primordial power spectrum offer a compelling alternative explanation [48–50]. We show that the transient multi-field dynamics in Higgs-R^2 inflation naturally generate features in the primordial curvature spectrum at large-intermediate scales, offering a potential primordial origin for the low-ℓ suppression without relying on ad-hoc potentials. By performing a full numerical integration of the background and perturbations, we identify two qualitatively distinct regimes: one in which isocurvature modes survive until the end of inflation ($\xi_h \ll 1$), and one in which a transient turning induces features while ensuring that isocurvature is strongly suppressed by the end ($\xi_h \sim \mathcal{O}(0.1)$). We compute the resulting CMB TT, TE, and EE spectra and discuss their implications for current observations.

This paper is organized as follows. In Section 2 we review the Higgs–R^2 model in the Einstein frame and study the background evolution. Section 3 discusses the evolution of linear perturbations. Section 4 presents the numerical results for the primordial spectra, and Section 5 explores the implications for the CMB observables. We summarize our conclusions in Section 6. Throughout this work we assume a spatially flat FLRW background

$$\mathrm{d}s^2 = -\mathrm{d}t^2 + a^2(t)\,(\mathrm{d}x^2 + \mathrm{d}y^2 + \mathrm{d}z^2), \tag{1.1}$$

and use natural units with $c = \hbar = G = M_p = 1$.

2 Multi-field Higgs-R^2 inflation

Our starting point is the Higgs-R^2 model [30, 33, 36] in the Jordan frame in its most general form, i.e., the theory of Higgs inflation [34] augmented by an R^2 term, whose action is given by

$$S_J[g_{\mu\nu}\,,\mathcal{H}] = \int \mathrm{d}^4x\sqrt{-g_J}\left[\frac{1}{2}\left(1+2\xi_h|\mathcal{H}|^2\right)R_J + \xi_s R_J^2 - g_J^{\mu\nu}(D_\mu\mathcal{H})^\dagger(D_\nu\mathcal{H}) - \lambda|\mathcal{H}|^4\right] \tag{2.1}$$

where the variables defined in the Jordan frame are denoted by the subscript J. The field $\mathcal{H}$ represents the Higgs doublet with a non-minimal coupling ξ_h, which is necessary for $\mathcal{H}$ to drive inflation, while λ is the quartic coupling constant and $D_\mu\mathcal{H}$ is the covariant derivative of the SM Higgs sector, which includes interactions with the gauge fields:

$$D_\mu\mathcal{H} = \left(\partial_\mu - \frac{ig}{2}\tau_a W^a{}_\mu + \frac{ig'}{2}B_\mu\right)\mathcal{H}\,. \tag{2.2}$$

The fields W^a_μ and B_μ represent the gauge fields of the $SU(2)$ and $U(1)$ groups, with their respective coupling constants g and g', while τ_a are the $SU(2)$ generators. It is customary to define the Higgs doublet $\mathcal{H}$ in the unitary gauge such that $\mathcal{H}$ is parameterized by a single field h:

$$\mathcal{H} = \frac{1}{\sqrt{2}}\begin{pmatrix} 0 \\ h + v_{\rm ew}\end{pmatrix}\,, \tag{2.3}$$

where $v_{\rm ew} \approx 246\,\text{GeV}$ is the electroweak energy scale. In this gauge, and considering that $h \gg v_{\rm ew}$, the action of the model can be rewritten as [30]

$$S_J[g_{\mu\nu}\,, h] = \int \mathrm{d}^4\sqrt{-g_J}\left[\frac{1}{2}\left(1+\xi_h h^2\right)R_J + \xi_s R_J^2 - \frac{1}{2}g_J^{\mu\nu}(\partial_\mu h)(\partial_\nu h) - \frac{\lambda}{4}h^4\right]\,, \tag{2.4}$$

where we have omitted interactions with the gauge fields. It is well established that this model is a natural extension of Higgs inflation that solves the large coupling constant problem [36]. The Higgs model requires a coupling constant $\xi_h \sim \mathcal{O}(10^4)$ to render the model compatible with CMB observables; however, it suffers from the strong coupling problem [34, 51, 52]. This problem arises because the Higgs field becomes strongly coupled at the electroweak scale, causing a loss of perturbative unitarity well below the usual Planck scale [36]. The cutoff scale is $\Lambda_{\rm UV} = M_p/\xi_h$, which casts doubt on the model's predictions. For $\xi_h \sim \mathcal{O}(10^4)$, the energy scale is of the order of $\Lambda_{\rm UV} \sim 10^{14}$, which is lower than the energy scale during inflation. However, the inclusion of the R^2 term naturally raises the model's cutoff to the Planck scale, thereby restoring its perturbative nature [30, 36]. The model (2.4) features two degrees of freedom: the field h and a scalar degree of freedom arising from R_J^2, known as the scalaron. Both fields are dynamic and contribute to the expansion history of the universe. This dynamics is more easily understood by rescaling the spacetime metric $g_{\mu\nu}$ via a conformal transformation $\Omega^2(x)$, so that the action (2.4) adopts the standard Einstein-Hilbert form plus an action for two scalar fields ϕ and h [53]. The conformal transformation that allow us to write (2.4) in the Einstein frame is $\Omega^2(x) = e^{-\alpha\phi}$, with $\alpha = \sqrt{2/3}$ and ϕ being the scalaron field [30]. The resulting action is

$$S_J \to S_E = \int \mathrm{d}^4x\sqrt{-g}\left[\frac{1}{2}R - \frac{1}{2}g^{\mu\nu}(\partial_\mu\phi)(\partial_\nu\phi) - \frac{1}{2}e^{-\alpha\phi}g^{\mu\nu}(\partial_\mu h)(\partial_\nu h) - V(\phi\,, h)\right]\,, \tag{2.5}$$

where the scalar potential $V(\phi\,, h)$ depends on both fields in the Einstein frame and is defined as

$$V(\phi\,,h) = e^{-2\alpha\phi}\left[\frac{1}{16\xi_s}\left(e^{\alpha\phi} - 1 - \xi_h\, h^2\right)^2 + \frac{\lambda}{4}\, h^4\right]. \tag{2.6}$$

The non-canonical kinetic term of h defines a non-trivial field-space metric G_{IJ} with non-vanishing components

$$G_{\phi\phi} = 1\,, \quad G_{hh} = e^{-\alpha\phi}\,. \tag{2.7}$$

This type of model, featuring a non-canonical kinetic term and two scalar fields, is well known and has been widely studied in the literature [9, 11, 12, 26, 54, 55], exploring various simple forms of the inflationary potential. By this, we refer to inflationary potentials that can typically be factorized as a sum of single-field potentials $V(\phi\,,\chi) = U(\phi) + W(\chi)$, or as a product $V(\phi\,,\chi) = U(\phi)W(\chi)$. The potential (2.6) is more involved in this sense, as it is not factorizable either as a sum or a product of individual potentials depending solely on ϕ or h. Furthermore, this model presents three parameters: λ, ξ_h, and ξ_s. According to [30], there are three cases that yield inflation at the energy scale $\phi \gg M_p$:

1. $\xi_h > 0\,, \xi_s > 0\,, \lambda > 0$
2. $\xi_h < 0\,, \xi_s > 0\,, \lambda > 0$
3. $\xi_h < 0\,, \xi_s > 0\,, \lambda < 0$

In all three cases, the inflationary dynamics effectively reduces to a single-field scenario for $\xi_h \gg 1$, as the isocurvature mode becomes heavy enough to be integrated out. This reduction in inflationary dynamics can be understood via the valley-approach, which we briefly demonstrate in Appendix A. The first case corresponds to a mixture between the Higgs field h and the scalaron ϕ; the inflaton potential is given by (A.2). In the second case, inflation is driven solely by the scalaron ϕ, while the third corresponds to the metastable EW vacuum. On the other hand, if $\xi_s \gg \xi_h^2/\lambda$, inflation is of the R^2-type, whereas in the opposite case, inflation is predominantly driven by the Higgs field h [30]. However, if no hierarchy exists among the parameters, it is ensured that both ϕ and h contribute to the inflationary dynamics and the generation of perturbations for $\xi_h \gg 1$. This case is known as the standard parameter space of the Higgs-R^2 model, where multi-field effects are known to be absent [31–33].

In this work, we explore the case $\xi_h > 0\,, \xi_s > 0\,, \lambda > 0$ with a parameter space satisfying $\xi_h \sim \lambda\xi_s \lesssim \mathcal{O}(0.1)$, such that isocurvature modes and their primordial features are not negligible during inflation. This condition ensures that the isocurvature mode is not too heavy to be excited during inflation, making its evolution relevant for primordial perturbations. The values of the parameters, beyond playing a role in the generation of isocurvature modes, impact the shape of the potential (2.6). In Fig. 1, we display the structure of the potential for two different parameter spaces. For a more detailed analysis of the potential shape and its consequences on field-space trajectories, we recommend Ref. [33].

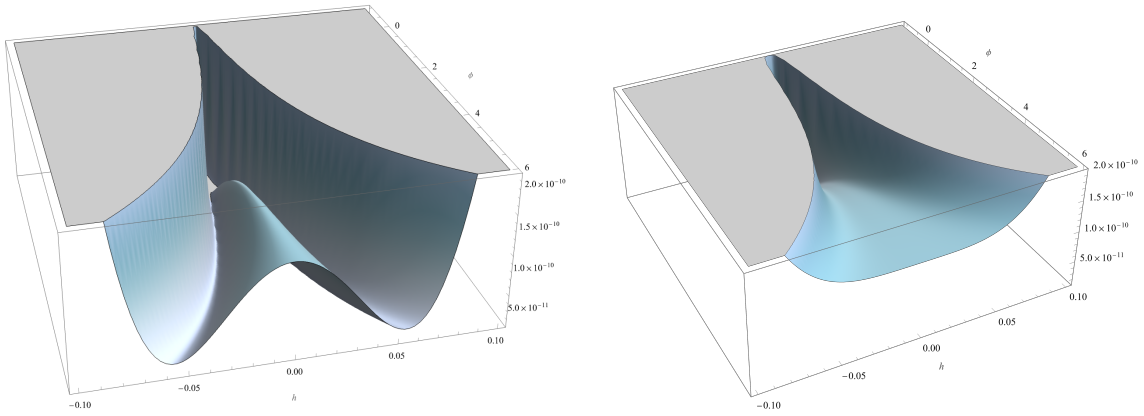

Figure 1. Scalar potential $V(\phi\,,h)/M_p^4$ in the Einstein frame. Left panel: Potential (2.6) using the standard parameter space $\lambda = 0.13$, $\xi_h = 4000$ and $\xi_s \simeq 10^8$. The potential exhibits a two-valley structure and a ridge at $h = 0$. Right panel: The same potential (2.6) but for a coupling $\xi_h = 0.1$. We observe that the valley and ridge structure disappears in the limit $\xi_h \ll 1$.

2.1 Background dynamics

To characterize the system's evolution in multi-field inflation models, it is customary to employ a covariant field-space formalism [27, 56–58]. The equations of motion for the fields ϕ, h are derived directly from (2.5). Using the covariant field-space approach and the metric (1.1), these are written as

$$D_t\dot{\phi}^I + 3H\dot{\phi}^I + G^{IJ}V_J = 0\,, \tag{2.8}$$

where D_t is the covariant directional derivative along t, defined acting on an arbitrary field-space vector A^I as $D_tA^I = \dot{\phi}^J\nabla_J A^I = \dot{A}^I + \Gamma^I{}_{JK}\,\dot{\phi}^J\,A^K$, while the Christoffel symbols are evaluated in terms of G_{IJ} and its derivatives via the expression $\Gamma^I{}_{JK} = G^{IM}(\partial_J G_{KM} + \partial_K G_{JM} - \partial_M G_{JK})/2$, with $\partial_J G_{KM} = \partial G_{KM}/\partial\phi^J$. For the metric (2.7), the non-vanishing components of $\Gamma^I{}_{JK}$ are

$$\Gamma^{\phi}{}_{hh} = \frac{\alpha}{2}e^{-\alpha\phi}\,, \quad \Gamma^{h}{}_{\phi h} = \Gamma^{h}{}_{h\phi} = -\frac{\alpha}{2}\,. \tag{2.9}$$

In a spacetime given by the FLRW metric (1.1), and assuming that the scalar fields are homogeneous, $\phi = \phi(t)$ and $h = h(t)$, the equations of motion (2.8) satisfied by the fields (ϕ, h) are given by

$$\ddot{\phi} + 3H\dot{\phi} + V_\phi = -\frac{\alpha}{2}e^{-\alpha\phi}\dot{h}\,, \quad \ddot{h} + (3H - \alpha\dot{\phi})\dot{h} + e^{\alpha\phi}\,V_h = 0\,, \tag{2.10}$$

where, as usual, an overdot denotes ∂_t, the subscripts on the potential indicate derivatives, and $H(t)$ is the Hubble parameter given by $H = \dot{a}/a$, with $a(t)$ being the scale factor. The evolution and dynamics of H are governed by the Friedmann equations:

$$\dot{H} = -\frac{1}{2}\dot{\sigma}^2\,, \quad 3H^2 = \frac{1}{2}\dot{\sigma}^2 + V(\phi\,,h)\,, \tag{2.11}$$

where $\dot{\sigma}^2 = G_{IJ}\dot{\phi}^I\dot{\phi}^J = \dot{\phi}^2 + e^{-\alpha\phi}\dot{h}^2$. The numerical solution of Eqs. (2.10) and (2.11), with an appropriate choice of initial conditions, provides the background trajectory. To discuss the features of said trajectory and the field-space geometry, it is useful to define the tangent vector T^I and the normal vector N^I to the trajectory as $T^I = \dot{\phi}^I/\dot{\sigma}$ and $N^I = \sqrt{\det G}\,\epsilon_{IJ}T^J$, where ϵ_{IJ} is the fully antisymmetric Levi-Civita symbol, and $\det G$ is the determinant of the metric (2.7). Explicitly, for the model (2.4), these vectors are given by

$$T^I = \frac{(\dot{\phi}\,,\dot{h})}{\dot{\sigma}}\,, \quad N^I = \frac{e^{\alpha\phi/2}}{\dot{\sigma}}\,(-e^{-\alpha\phi}\dot{h}\,,\dot{\phi})\,. \tag{2.12}$$

The vector T^I defines the direction parallel to the trajectory (adiabatic) of any field-space vector A^I, while N^I defines the first normal component (isocurvature) of A^I [27]. In this way, these vectors allow us to decompose any vector A^I into its adiabatic component A_σ and isocurvature component A_s as $A^I = A_\sigma T^I + A_s N^I$. Furthermore, the vector T^I offers an alternative way to write the equation of motion (2.8) as two independent equations: $\ddot{\sigma} + 3H\dot{\sigma} + V_\sigma = 0$ and $D_t T^I = -H\eta_\perp N^I$, where we have defined $V_\sigma = T^I V_I$ and $V_N = N^I V_I$ as the projections of $\partial_I V = V_I$ along the adiabatic and isocurvature directions, respectively. The parameter $\eta_\perp$ is known as the turning rate and indicates the rate of change of T^I along the N^I direction. If $\eta_\perp = 0$, the vectors (2.12) remain covariantly constant along the classical trajectory, whereas if $\eta_\perp \neq 0$, the vectors T^I and N^I can rotate to the right or left, depending on the sign of $\eta_\perp$. It is important to note that if the trajectory $\phi^I(t)$ is a geodesic in field space ($D_t\dot{\phi}^I = 0$), the turning rate vanishes. Moreover, this parameter is responsible for sourcing the mixing between the adiabatic and isocurvature modes of the primordial perturbations and parameterizes the interaction between them; thus, for geodesic motion in field space, both perturbations evolve independently (see Section 3).

Characterizing the dynamics of this type of model involves a slow-roll analysis analogous to that of single-field inflation models. We can define the slow-roll parameters as

$$\epsilon = -\frac{\dot{H}}{H^2}\,, \quad \eta^I = -\frac{D_t\,\dot{\phi}^I}{H\dot{\sigma}}\,, \tag{2.13}$$

where ϵ is the usual slow-roll parameter, while η^I is a vector in field space containing information about the second slow-roll parameter. We decompose η^I into its adiabatic and isocurvature components $\eta^I = \eta_{||}T^I + \eta_\perp N^I$, where $\eta_{||} = \eta^I T_I$ and $\eta_\perp = \eta^I N_I$ are given by

$$\eta_{||} = -\frac{\ddot{\sigma}}{H\dot{\sigma}}\,, \quad \eta_\perp = \frac{V_N}{H\dot{\sigma}}\,. \tag{2.14}$$

It is clear that the component $\eta_{||}$ is the counterpart of the second slow-roll parameter in single-field models, while $\eta_\perp$ is the turning rate parameter appearing in the equation $D_t T^I = -H\eta_\perp N^I$. The slow-roll conditions in these models are given by $\epsilon \ll 1$ and $|\eta_{||}| \ll 1$, which is equivalent to $\ddot{\sigma} \ll |H\dot{\sigma}|$. These conditions do not imply a small turning rate $\eta_\perp \ll 1$; therefore, $\eta_\perp \gtrsim 1$ is compatible with the slow-roll approximation. Using the explicit form of N^I, we can construct the projection of the gradient of the potential (2.6) along the isocurvature direction:

$$V_N = N^I V_I = \frac{e^{\alpha\phi/2}}{\dot{\sigma}}(V_h\dot{\phi} - e^{-\alpha\phi}\dot{h}V_\phi)\,. \tag{2.15}$$

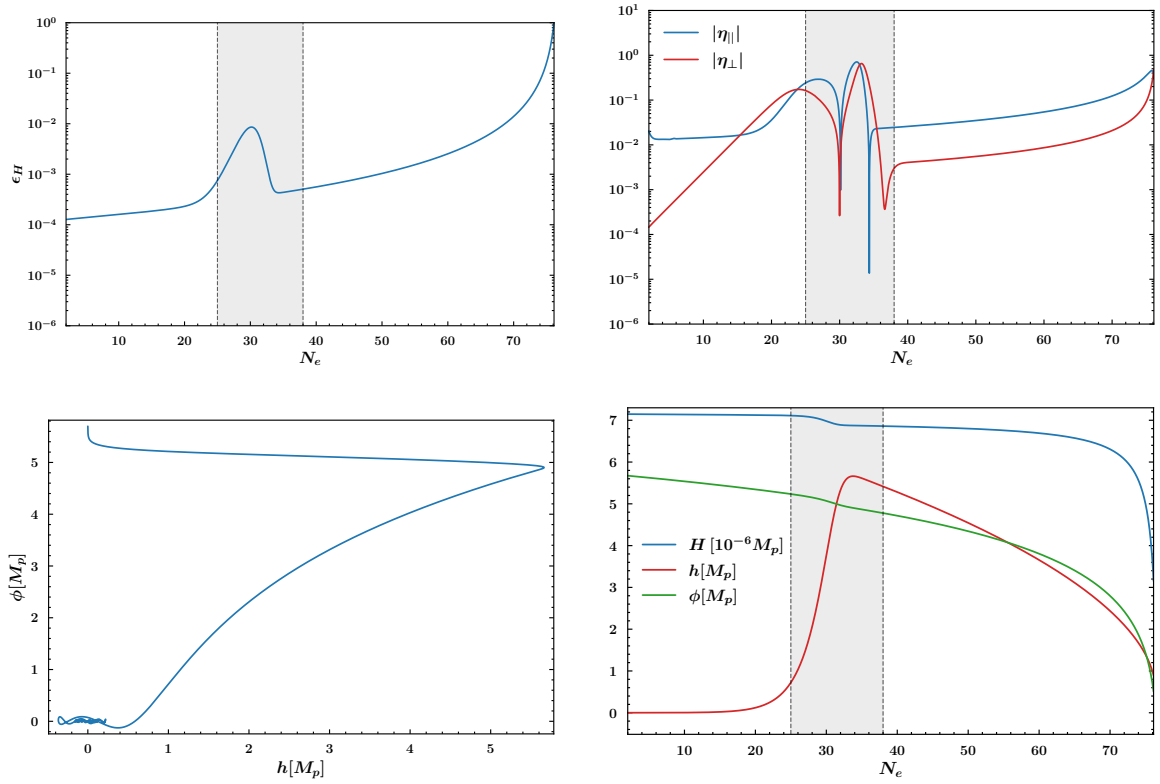

Figure 2. Evolution of the slow-roll parameter ϵ_H, the turning rate parameter $\eta_\perp$, and the parameter $\eta_{||}$, along with the field-space trajectory and background variables (H, ϕ, h) as a function of the number of e-folds N_e. We consider the parameter set $\xi_h = 0.1$, $\lambda = 10^{-10}$, and $\xi_s = 4 \times 10^8$, with initial conditions $\phi_0 = 5.7$ and $h_0(\phi_0) = 10^{-4}$ in Planck units. It is observed that, although inflation begins in a slow-roll regime ($\epsilon_H \ll 1$), the initial conditions produce transient peaks associated with turns in the field-space trajectory.

This allows us to write the model's turning rate as

$$\eta_\perp = \frac{e^{\alpha\phi/2}}{H\dot{\sigma}^2}\left(V_h\dot{\phi} - e^{-\alpha\phi}\,\dot{h}V_\phi\right). \tag{2.16}$$

Within the valley-approach, the turning rate and the orthonormal vectors to the field-space trajectory are given in (A.4). In the standard parameter space and within the valley-approach, the turning rate is negligible, but for the parameter space satisfying $\xi_h \sim \lambda\xi_s$, the turning rate is of the order $\eta_\perp \sim \mathcal{O}(0.1)$. Nevertheless, for a proper understanding of the background evolution, it is convenient to perform a numerical analysis of both the background variables and the perturbations. To this end, it is convenient to use the number of e-folds N_e as the time parameter, given the relation $\mathrm{d}N_e = H\mathrm{d}t$. In this case, equations (2.10) and (2.11) take the form

$$\phi'' + (3-\epsilon)\,\phi' + \frac{V_\phi}{H^2} = -\frac{\alpha}{2}e^{-\alpha\phi}h',$$

$$h'' + (3-\epsilon-\alpha\phi')\,h' + e^{\alpha\phi}\frac{V_h}{H^2} = 0,$$

$$H^2 = \frac{V}{3-\epsilon}\,. \tag{2.17}$$

where a prime denotes ∂_{N_e}, while the slow-roll parameter ϵ in terms of e-folds is written as

$$\epsilon = -\frac{H'}{H} = \frac{1}{2}(\phi'^2 + e^{-\alpha\phi}h'^2)\,, \tag{2.18}$$

and the turning rate (2.16) as a function of N_e is given by

$$\eta_\perp = \frac{e^{\alpha\phi/2}}{\sigma_N^2}\left(V_h\phi' - e^{-\alpha\phi}\,V_\phi h'\right)\,, \tag{2.19}$$

where $\sigma_N^2 = H^2(\phi'^2 + e^{-\alpha\phi}h'^2)$. Once the model parameters and suitable initial conditions have been specified, we can proceed to numerically integrate the system of equations (2.17) to obtain the relevant background quantities.

With these quantities, we can proceed to analyze the primordial perturbations of the model. Following Ref. [59], the analysis and evolution of linear primordial perturbations are determined by three functions: the Hubble parameter $H(N)$, the turning rate $\eta_\perp(N)$, and the mass of the isocurvature mode $m_{\rm iso}^2(N)$. In Fig. 2, we display the numerical solution for the background; specifically, we show the behavior of $\epsilon_H(N)$, $\phi(N)$, $h(N)$, $H(N)$, $\eta_\perp(N)$, and $\eta_{||}(N)$ given the initial condition $\phi_0 = 5.7$ in Planck units. The initial condition of the field h determines the starting position on the potential. If $h_0 = h_0^{\rm valley}$ is given by condition (A.1), inflation begins exactly within one of the potential valleys; if $h_0 \ll 1$, multi-field effects associated with the fall from the ridge at $h = 0$ towards one of the valleys are guaranteed [33]. As an example, we show the background for the initial condition $h_0 = 10^{-4}M_p$. We can observe some important features in the background behavior. Around $N_e \simeq 25 - 35$, a turn in the field-space trajectory occurs, which is reflected in the parameters $\eta_\perp$ and ϵ_H. The small increase in ϵ_H represents a temporary deviation from the slow-roll regime associated with this turn. Although inflation is not interrupted ($\epsilon_H \ll 1$ at all times), this behavior can leave observable imprints on the primordial power spectrum of $\mathcal{R}_k$ (see Section 4.2). This type of behavior is typical of potentials with local features ("bumps" or "dips") designed to induce ultra-slow-roll phases ($\epsilon_H \to 0$) and amplify the primordial spectrum to values of $\mathcal{P}_\mathcal{R}(k) \sim 10^{-2} - 10^{-1}$, which are necessary for the formation of primordial black holes (PBHs) [60]. Such mechanisms can also occur in multi-field models with transient turns in field space [25, 45, 46]; however, in our case, the change in trajectory is not sharp enough to amplify the spectrum up to the PBH production regime.

3 Primordial perturbations

When studying primordial perturbations at linear or quadratic order in multi-field inflation models, it is advisable to adopt a covariant approach with respect to gauge transformations in field space. This formalism was developed in detail in Ref. [56] for an arbitrary field space. In this paper, we neglect vector perturbations and focus primarily on scalar primordial perturbations. From a covariant perspective, the strategy is to employ the covariant perturbation Q^I instead of the coordinate perturbation $\delta\phi^I(t\,,\mathbf{r}) = \phi^I(t\,,\mathbf{r}) - \bar{\phi}^I(t)$, where

$\bar{\phi}^I(t)$ is the classical background trajectory satisfying (2.8). The values of $\bar{\phi}^I$ and ϕ^I at a fixed spacetime point P can be connected via a unique geodesic in field space parameterized by ε, which relates the initial value of ϕ^I to the tangent vector at P. The initial conditions are set at $\varepsilon = 0$, such that

$$\phi^I(\varepsilon = 0) = \bar{\phi}^I\,, \quad Q^I = \left.\frac{\mathrm{d}\phi^I}{\mathrm{d}\varepsilon}\right|_{\varepsilon=0}\,. \tag{3.1}$$

At second order in perturbations, one finds the expansion relating Q^I to the perturbation $\delta\phi^I$:

$$\delta\phi^I = \phi^I - \bar{\phi}^I = Q^I - \frac{1}{2}\,\Gamma^I{}_{JK}\,Q^J Q^K + \cdots\,. \tag{3.2}$$

Since both $\delta\phi^I$ and Q^I are field-space vectors, we can decompose them into their adiabatic component Q_σ and isocurvature component Q_s as $Q^I = Q_\sigma T^I + Q_s N^I$, where a priori both components are dynamic. On the other hand, the study of spacetime perturbations and their mixing with Q^I is simplified by using the ADM form [61, 62] of the metric (1.1):

$$\mathrm{d}s^2 = -N^2\mathrm{d}\phi^2 + \gamma_{ij}\,(N^i\mathrm{d}\phi + \mathrm{d}x^i)(N^j\mathrm{d}\phi + \mathrm{d}x^j)\,, \tag{3.3}$$

where $\mathrm{d}\phi$ is a time parameterization, N is the lapse function, N^i is the shift vector, and γ_{ij} is the induced 3-metric on the hypersurface Σ_t. The rationale behind the ADM formalism in the study of cosmological perturbations is to expand the action (2.5) to second order in a power series of the perturbations. This approach was introduced by Maldacena [62] for single-field inflation models. Since N and N^i are non-dynamical Lagrange multipliers, the 3-metric γ_{ij} contains the physical information of the system. By fixing a time parameterization and choosing the shift vector, we fix N and N^i, which is achieved by choosing a gauge. In inflation and perturbation theory, it is common practice to employ the spatially flat gauge, where $\gamma_{ij}^{\mathrm{flat}} = a^2(t)\delta_{ij}$, and all dynamics are contained within the perturbation $\delta\phi^I$. This gauge has been widely used in the literature [6, 7, 14, 28, 63] and has the advantage that the components of the perturbation $\delta\phi^I$ are Mukhanov-Sasaki (MS) variables, thus satisfying an MS-type equation [6, 10, 64, 65]. However, in this work, we choose to work with the comoving gauge, defined as [15, 66–68]:

$$\gamma_{ij}^{\mathrm{com}} = a^2(t)e^{2\mathcal{R}}\delta_{ij}\,, \quad T_I Q^I = 0\,. \tag{3.4}$$

where $\mathcal{R}$ is the gauge-invariant comoving curvature perturbation [69]. The main feature of this gauge is that the adiabatic component of Q^I vanishes, but the isocurvature part is $Q_s = N_I Q^I$. Consequently, in the comoving gauge, the perturbations are $\mathcal{R}$ and Q_s. The action at second order in these variables is written as

$$S^{(2)} = \int \mathrm{d}^4x\, a^3 \left[\epsilon\left(\dot{\mathcal{R}}^2 - a^{-2}\delta^{ij}\partial_i\mathcal{R}\partial_j\mathcal{R}\right) + \frac{1}{2}\left(\dot{Q}_s^2 - a^{-2}\delta^{ij}\partial_i Q_s\partial_j Q_s - m_{\mathrm{iso}}^2 Q_s^2\right)\right.$$
$$\left. +2H\eta_\perp\sqrt{2\epsilon}\,Q_s\dot{\mathcal{R}}\right]\,, \tag{3.5}$$

where ϵ is the slow-roll parameter given in (2.13), while $m^2_{\rm iso}$ is the effective mass of the isocurvature mode Q_s, given by

$$m^2_{\rm iso} = N^I N^J \nabla_I V_J + H^2 \epsilon\, R_{\rm fs} - (H\eta_\perp)^2\,, \tag{3.6}$$

where $R_{\rm fs} = -1/3$ is the field-space Ricci scalar of the model in units of M_p, defined via G_{IJ} (2.7). The first term $V_{NN} = N^I N^J \nabla_I V_J$ represents the usual mass contribution given the potential (2.6):

$$\begin{aligned} V_{NN} &= N^I N^J \nabla_I V_J = N^I N^J (\partial_I \partial_J V - \Gamma^K{}_{IJ} \partial_K V) \\ &= \frac{1}{\dot\sigma^2}\left(e^{\alpha\phi}\dot\phi^2 V_{hh} + e^{-\alpha\phi}\dot h^2 V_{\phi\phi} - 2\dot\phi\,\dot h V_{h\phi} - \frac{\alpha}{2}(\dot\phi^2 V_\phi + 2\dot\phi\,\dot h V_h)\right)\,, \end{aligned} \tag{3.7}$$

which depends on the derivatives of the potential (2.6) and the background dynamics. However, this can be considerably simplified if we take into account the valley-approach (A.1) and the results in (A.4). By explicitly substituting the form of N^I and the potential, and taking (A.1) into account, we obtain

$$V_{NN} \simeq \frac{\xi_h(24\lambda\xi_s + \xi_h(1+6\xi_h))}{\lambda\xi_s}\, H^2\,. \tag{3.8}$$

The second term in (3.6) represents a contribution from the curved geometry of the field space, while the third term yields a negative contribution to the mass and is a correction due to the turn of the classical trajectory induced by (2.16). We observe that even if the turning rate is zero, multi-field effects do not vanish, as the second term in (3.6) arising from the field-space geometry is non-trivial. Under the approximation (A.4), the mass $m^2_{\rm iso}$ becomes

$$\frac{m^2_{\rm iso}}{H^2} \simeq \frac{\xi_h(24\lambda\xi_s + \xi_h(1+6\xi_h))}{\lambda\xi_s} - \frac{\epsilon}{3} - \frac{\tilde\xi^2}{1+\tilde\xi^2}\,, \tag{3.9}$$

where $\tilde\xi^2 = \xi_h/6(\xi_h^2 + 4\lambda\xi_s)$. We observe that in the valley-approach, the mass of the Q_s mode takes a simplified form, and the ratio $m^2_{\rm iso}/H^2$ is effectively constant. This facilitates the search for analytical solutions to the equation for Q_s. On the other hand, if $\xi_h \gg 1$, the isocurvature mode is heavy and the turning rate is negligible, allowing us to ignore the evolution of Q_s. If we take $\xi_h \sim \lambda\xi_s$, the value of $m^2_{\rm iso}$ is close to H^2; consequently, the Q_s mode becomes light and the turning rate becomes significant. In this scenario, the single-field approximation fails, and one must adopt a quasi-single field inflation (QSFI) scenario [16, 70], or numerically solve the equations for the modes $\mathcal{R}_k$ and Q_s, going beyond the single-field slow-roll approximation [32].

3.1 Evolution of adiabatic and isocurvature perturbations

The equations of motion for the perturbations $\mathcal{R}$ and Q_s are obtained by varying the action (3.5). In terms of cosmic time t and in Fourier space, these are given by:

$$\ddot{\mathcal{R}}_k + (3+\delta)H\dot{\mathcal{R}}_k + \frac{k^2}{a^2}\mathcal{R}_k = -\frac{2H\eta_\perp}{\sqrt{2\epsilon}}[\dot Q_s + (3 - \xi_\perp - \eta_{||})HQ_s] \tag{3.10}$$

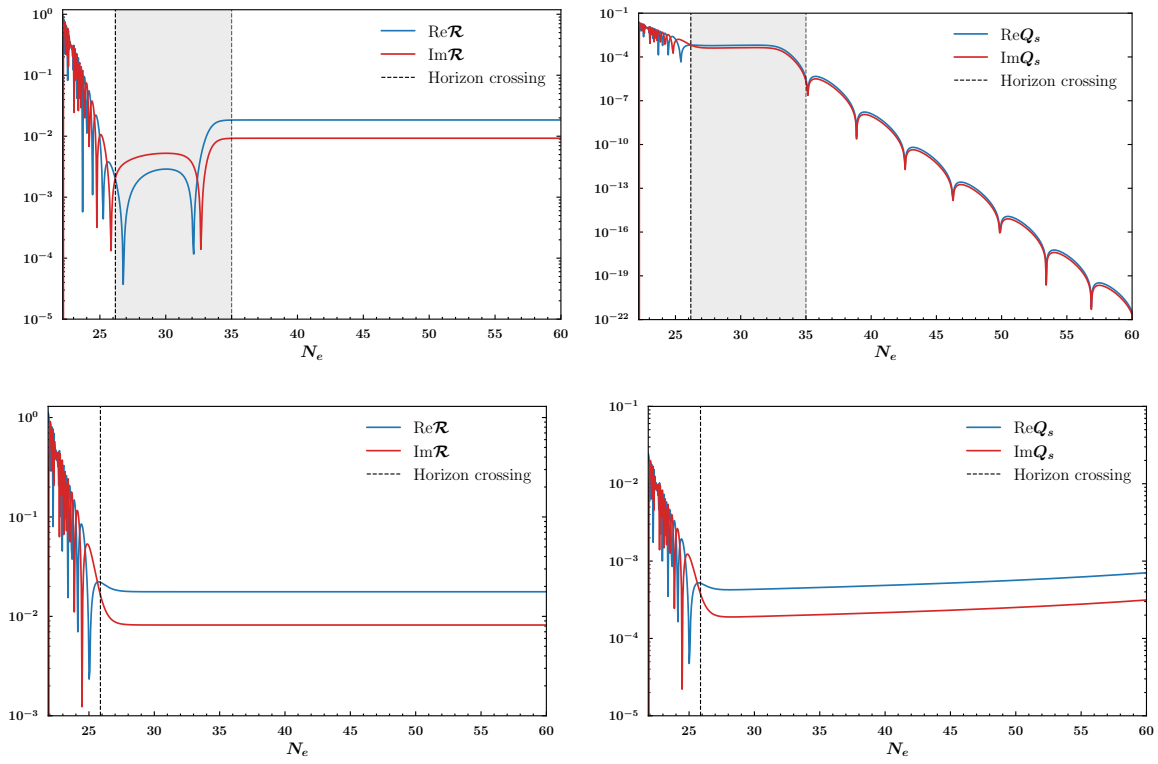

Figure 3. Numerical solution of equations (3.13) and (3.14) for the space parameter $\xi_h = 0.1$ (top panel) and $\xi_h = 10^{-9}$ (bottom panel) with $\lambda = 10^{-10}$ and $\xi_s = 4 \times 10^8$ fixed. We also fixed the initial conditions to $\phi_0 = 5.7$ and $h_0 = 10^{-4}$ in Planck units. The vertical dashed line indicates horizon crossing for the pivot scale $k_* = 0.05\,\mathrm{Mpc}^{-1}$.

$$\ddot{Q}_s + 3H\dot{Q}_s + \left(\frac{k^2}{a^2} + m_{\rm iso}^2\right) Q_s = 2H\eta_\perp \sqrt{2\epsilon}\dot{\mathcal{R}}_k \,, \tag{3.11}$$

where $\delta = 2(\epsilon - \eta_{||})$ and $\xi_\perp = -\dot{\eta}_\perp / H\eta_\perp$. The action (3.5) and equations (3.10) and (3.11) are exact; that is, no approximations were made in their derivation. Generally speaking, we can integrate the modes $\mathcal{R}_k$ and Q_s on super-Hubble scales ($k \ll aH$) for $\eta_\perp \neq 0$. The equation for the isocurvature mode Q_s becomes

$$\ddot{Q}_s + 3H\dot{Q}_s + m_{\rm eff}^2 Q_s \simeq 0 \,, \tag{3.12}$$

where the effective mass is given by $m_{\rm eff}^2 = m_{\rm iso}^2 + 4(H\eta_\perp)^2$, with $m_{\rm iso}^2$ defined in (3.6). In this case, the turning rate parameter always makes a positive contribution to the mass of the Q_s mode, acting as a source for the adiabatic mode such that $\dot{\mathcal{R}}_k \simeq -\sqrt{2}H\eta_\perp Q_s/\sqrt{\epsilon}$. For $\eta_\perp = 0$, it is clear that the mode $\dot{\mathcal{R}}_k$ decays exponentially, and thus $\mathcal{R}_k$ converges to a constant value, recovering the standard single-field inflation result. It is worth noting that the mass of the Q_s mode does not depend on the super-Hubble evolution of the adiabatic mode, so it can be calculated independently. Thus, the mass $m_{\rm iso}^2$ is solely a function of the background variables and contains all the relevant physical information for Q_s.

To visualize this behavior and track the full evolution of the $\mathcal{R}_k$ and Q_s modes on super-Hubble scales, it is convenient to perform a numerical analysis of the perturbations. As with the background dynamics, it is more efficient to numerically integrate equations (3.10) and (3.11) in terms of N_e:

$$\mathcal{R}_k'' + \left(1 - \epsilon + 2\frac{\mathrm{d}\log z}{\mathrm{d}N}\right)\mathcal{R}_k' + \left(\frac{k}{aH}\right)^2 \mathcal{R}_k = -\frac{2\eta_\perp}{\sqrt{2\epsilon}}[Q_s' + (3 - \xi_\perp - \eta_{||})Q_s]\,, \tag{3.13}$$

$$Q_s'' + (3-\epsilon)Q_s' + \left[\left(\frac{k}{aH}\right)^2 + \frac{m_{\rm iso}^2}{H^2}\right] Q_s = 2\sqrt{2\epsilon}\,\eta_\perp \mathcal{R}_k'\,, \tag{3.14}$$

where $z = a\sqrt{2\epsilon}$, with ϵ given by (2.18). We impose the Bunch-Davies vacuum as the initial condition for the modes $\mathcal{R}_k$ and Q_s, taking into account that the Mukhanov-Sasaki variables u_k and v_k are defined as $u_k = z\mathcal{R}_k$ and $v_k = aQ_s$. One must ensure that for each mode, the perturbations are initially deep inside the horizon ($k \gg aH$). If $N_{\rm hc}$ is the e-fold corresponding to the horizon crossing of the mode, $k = aH$, we start the evolution 5 e-folds earlier, i.e., $N_{\rm ini} = N_{\rm hc} - 5$. This guarantees that for each mode k, the perturbations are well within the horizon at the start of the integration. In terms of the number of e-folds, the initial conditions for $\mathcal{R}_k$ and Q_s are given by

$$\mathcal{R}_k(N_{\rm ini}) = \frac{1}{z(N_{\rm ini})\sqrt{2k}}\,, \quad Q_s(N_{\rm ini}) = \frac{1}{a_0\sqrt{2k}}\,, \tag{3.15}$$

where $a_0 = a(N_{\rm ini})$ is the value of the scale factor at $N_{\rm ini}$. We separate the real and imaginary parts of equations (3.13) and (3.14), as well as the initial conditions (3.15), to achieve greater numerical stability in the solution. In Fig. 3, we display the evolution of the perturbations $\mathcal{R}_k$ and Q_s as a function of N_e for the pivot scale $k_* = 0.05\,\mathrm{Mpc}^{-1}$ and for two space parameters $\xi_h = 0.1$ and $\xi_h = 10^{-9}$. As observed for $\xi_h = 0.1$, the mode $\mathcal{R}_k$ continues to evolve after horizon crossing due to the turning rate $\eta_\perp$ in field space, until it eventually freezes out. This evolution is driven by the coupling between the $\mathcal{R}_k$ and Q_s modes via the turning rate parameter $\eta_\perp$. This transfer from the Q_s mode is consistent with the previous discussion. In contrast, the isocurvature mode Q_s evolves after crossing and is exponentially suppressed as a consequence of its effective mass $m_{\rm iso}^2 \gtrsim H^2$, limiting its late-time contribution as a source for $\mathcal{R}_k$. For the case $\xi_h = 10^{-9}$, the situations is identical to the single-field case: the adiabatic perturbation freezes out after horizon crossing since there is no coupling with isocurvature mode Q_s.

4 Primordial power spectra

We have mentioned that the background behavior shown in Fig. 2 triggers multi-field effects, which are reflected in the evolution of the primordial perturbations $\mathcal{R}_k$ and Q_s on super-Hubble scales (see Fig. 4). In particular, these effects can generate additional features in the primordial spectrum, depending on the value of the constant coupling ξ_h. Although the variables $\mathcal{R}_k$ and Q_s are convenient for integrating the perturbation equations, it is more useful to express the results in terms of the dimensionless isocurvature perturbation

$$\mathcal{S}_k \equiv \frac{H}{\dot{\sigma}} Q_s \,, \tag{4.1}$$

which allows for a direct comparison with observational literature. Super-Hubble evolution induces a correlation between the adiabatic mode $\mathcal{R}_k$ and the isocurvature mode $\mathcal{S}_k$. Therefore, the primordial spectrum is characterized by three functions:

$$\mathcal{P}_{\mathcal{R}}(k) = \frac{k^3}{2\pi^2} |\mathcal{R}_k|^2, \qquad \mathcal{P}_{\mathcal{S}}(k) = \frac{k^3}{2\pi^2} |\mathcal{S}_k|^2, \qquad C_{\mathcal{RS}}(k) = \frac{k^3}{2\pi^2} \mathrm{Re}(\mathcal{R}_k \mathcal{S}_k^*) \,. \tag{4.2}$$

The quantity $C_{\mathcal{RS}}(k)$ is known as the *cross-correlation spectrum* and quantifies the degree of correlation between both modes. From the adiabatic and isocurvature spectra, we can define the relative isocurvature fraction

$$\beta_{\rm iso}(k) = \frac{\mathcal{P}_{\mathcal{S}}(k)}{\mathcal{P}_{\mathcal{R}}(k) + \mathcal{P}_{\mathcal{S}}(k)} \,, \tag{4.3}$$

which can be compared with the most recent observational limits from Planck [5]. Additionally, the correlation between modes is parameterized via the correlation angle

$$\cos\Delta = \frac{C_{\mathcal{RS}}}{\sqrt{\mathcal{P}_{\mathcal{R}}\,\mathcal{P}_{\mathcal{S}}}} \,, \tag{4.4}$$

which takes values in the interval $(-1, 1)$ for each mode k. It is customary in the literature to evaluate these quantities at three representative scales: $k_{\rm low} = 0.002\,\mathrm{Mpc}^{-1}$, $k_* = 0.05\,\mathrm{Mpc}^{-1}$, and $k_{\rm high} = 0.1\,\mathrm{Mpc}^{-1}$, the same scales employed by the Planck analysis [5]. The presence of a non-zero cross-spectrum is a purely multi-field feature: the transfer $\mathcal{S}_k \to \mathcal{R}_k$ on super-Hubble scales is controlled by the turning rate parameter $\eta_\perp$, as follows from the evolution equation for $\dot{\mathcal{R}}_k$. Therefore, both the amplitude and shape of $C_{\mathcal{RS}}$ act as direct tracers of the field-space trajectory geometry. Observationally, a non-zero value of $C_{\mathcal{RS}}$ implies that the primordial spectrum cannot be described solely by the adiabatic and isocurvature amplitudes, but requires a relative phase between the modes. This effect can modify the CMB angular power spectra in specific ways through linear interference between the adiabatic and isocurvature terms, an aspect we will discuss in Sec. 5 using the obtained primordial spectrum as input for Boltzmann codes such as `CLASS` [71] [1].

4.1 Numerical results

Based on the numerical solutions for the background (Fig. 2) and perturbations (Fig. 4), we evaluate the primordial spectrum at the end of inflation, defined by the e-fold $N_{\rm end}$ such that $\epsilon_H(N_{\rm end}) = 1$. For each mode k, we identify the horizon crossing time $N_{\rm hc}$ via the condition $k = aH$, while $N_{\rm CMB}$ denotes the e-fold corresponding to the pivot scale $k_* = 0.05\,\mathrm{Mpc}^{-1}$, which we fix it in $N_{\rm CMB} = 50$ for all the cases. In this way, each k value is uniquely associated with a crossing instant during the inflationary evolution. To encompass both the observable CMB scales and the modes exiting the horizon in the final stages of inflation, we construct a logarithmic grid of 1000 k values in the interval $[k_{\rm min}, k_{\rm max}]$, where $k_{\rm min} = aH(N_{\rm hc} - 7)$ and $k_{\rm max} = aH(N_{\rm end} - 4)$. This range covers from $k \sim 10^{-6}\,\mathrm{Mpc}^{-1}$ to $k \sim 10^{19}\,\mathrm{Mpc}^{-1}$ and ensures that the power spectrum calculation incorporates modes experiencing the $\mathcal{S}_k \to \mathcal{R}_k$ transfer

[1] The public code can be found in the repository https://github.com/lesgourg/class_public.git.

throughout all dynamic stages of the model. We evaluate Eq. (4.2) at the end of inflation for each mode k; unlike the single-field case, it is not evaluated at horizon crossing because the power spectrum undergoes super-Hubble evolution for the parameter space of interest. This guarantees that the perturbation $\mathcal{R}_k$ has frozen out and that Q_s exhibits the expected exponential decay. Our approach covers two important cases: $\xi_h \ll 1$ and $\xi_h \sim \mathcal{O}(0.1)$; in both instances, we fix $\lambda = 10^{-10}$ and $\xi_s = 4 \times 10^8$. The initial condition is also set to $h_0 = 10^{-4} M_p$. Our results in this paper for the background, primoridal perturbations and the power spectrum can be produced by our numerical code which is available in GitHub repository. [2]

4.1.1 Case $\xi_h \ll 1$

This scenario simplifies both the isocurvature mass $m^2_{\rm iso}$ and the turning rate $\eta_\perp$ within one of the valleys. As discussed in Ref. [33], the potential loses its two-valley structure, which degenerates into a single valley centered at $h = 0$. Consequently, the dynamics may commence within the valley or precisely on the ridge, from where the field eventually oscillates and falls into the valley towards the potential minimum at $(0, 0)$. Within the valley, the turning rate vanishes ($\eta_\perp \to 0$) for $\xi_h \ll 1$, as shown in Appendix A.4, while the mass of the Q_s mode is given by

$$\frac{m^2_{\rm iso}}{H^2} \simeq -\frac{\epsilon}{3} \tag{4.5}$$

in accordance with Eq. (3.9). Thus, the mass remains light and negative during inflation. This causes the Q_s mode to grow on super-Hubble scales ($k \ll aH$). On the other hand, the fact that $\eta_\perp \simeq 0$ in this parameter space renders the perturbations statistically independent as long as this condition holds, since the generation of correlations and the energy transfer from the isocurvature to the curvature mode require the perturbations to be coupled via $\eta_\perp$. However, isocurvature modes are produced and survive until the end of inflation, owing to the lightness of the Q_s field. Consequently, both $\mathcal{R}_k$ and $\mathcal{S}_k$ evolve independently throughout the entire inflationary period. This behavior is displayed in Fig. 4. The top-left panel displays the evolution of the primordial spectra $\mathcal{P}_\mathcal{R}(k)$, $\mathcal{P}_\mathcal{S}(k)$, and $\mathcal{P}_\mathcal{T}(k)$ as a function of the number of e-folds N_e, evaluated at the pivot scale $k_* = 0.05\,\mathrm{Mpc}^{-1}$. At horizon crossing, the power spectrum of $\mathcal{R}_k$ freezes out as expected (since $\eta_\perp \simeq 0$), but $\mathcal{P}_\mathcal{S}(k)$ is not suppressed at the end of inflation, and its contribution remains non-zero. This is because the effective mass of the Q_s mode remains light throughout the evolution, in agreement with our analysis. The tensor spectrum remains practically unaltered, as there is no coupling between scalar and tensor degrees of freedom at linear order in perturbations. The top-right panel shows the primordial power spectrum at the end of inflation. As observed, the curvature power spectrum $\mathcal{P}_\mathcal{R}(k)$ exhibits no features; at large scales, its amplitude is of the order of 10^{-9}, while at small scales, it presents a suppression in magnitude. On the other hand, the isocurvature power spectrum is of the order of 10^{-11}. The bottom panels display the isocurvature fraction $\beta_{\rm iso}$ (left) and the cross-correlation $\cos\Delta$ (right) as a function of e-folds. The cross-correlation vanishes because the turning rate is negligible in this parameter space, but the isocurvature fraction is non-zero at the end of inflation, reaching a value of $\beta_{\rm iso} \approx 0.0101$ at the pivot scale $k_* = 0.05\,\mathrm{Mpc}^{-1}$.

[2] https://github.com/fpineda94/Higgs-R-2-inflation.git.

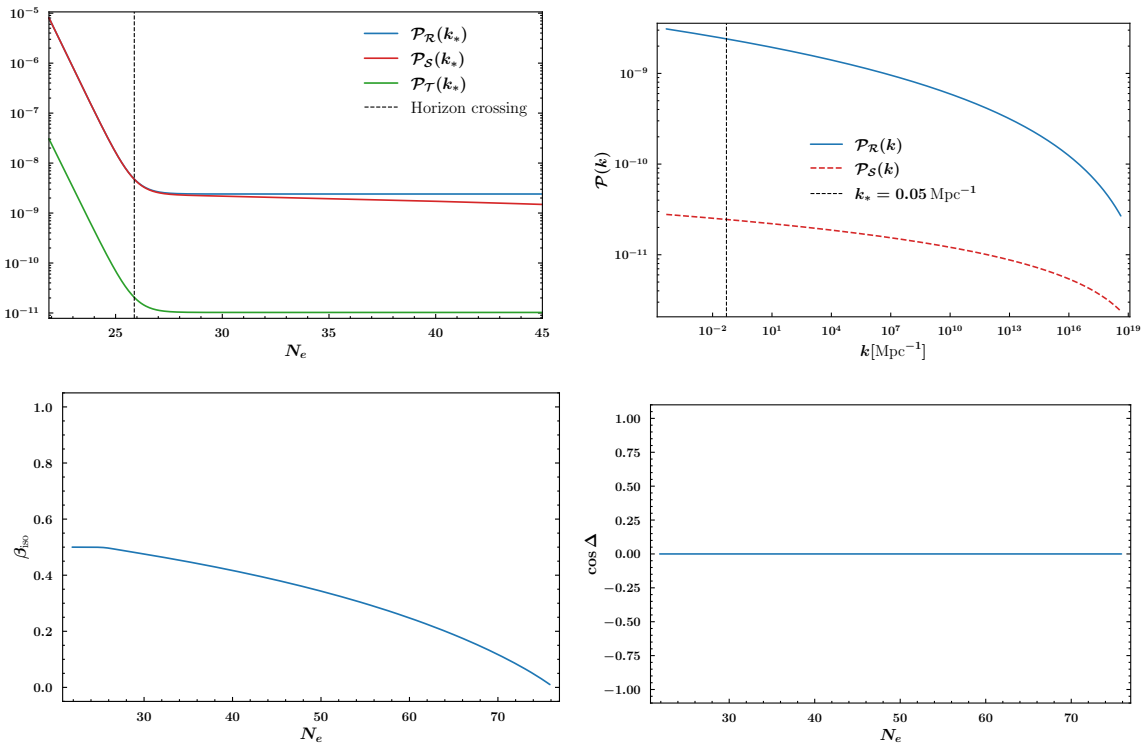

Figure 4. Primordial power spectrum for adiabatic (left panel) and isocurvature (right panel) perturbations evaluated at the end of inflation for $\xi_h = 10^{-9}$ and $\lambda = 10^{-10}$, $\xi_s = 4 \times 10^8$. We can see that the isocurvature perturbations remain non-zero at the end of inflation.

This value corresponds to an isocurvature contribution of the order of 1%, compatible with current limits from the Planck analysis on CDM isocurvature models $\beta_{\mathrm{iso}}(k_*) < 0.038$ at 95%) CL [5], although a precise comparison depends on the correlation and the spectral index of the isocurvature component. The absence of correlation simplifies the impact on the angular spectra, implying that the applicable observational bounds correspond to the uncorrelated Planck case. Furthermore, we verify that the inclusion of this fraction in `CLASS` does not generate significant discrepancies with the observed angular spectrum (see Section 5).

4.1.2 Case $\xi_h \sim \mathcal{O}(10^{-1})$

For the parameter space where $\xi_h \sim 0.1$, we observe a distinct phenomenological behavior compared to the small coupling limit. We find that the isocurvature component is strongly anti-correlated with the adiabatic mode at the moment of horizon crossing for the pivot scale. However, $\mathcal{P}_\mathcal{S}$ is fully suppressed during super-Hubble evolution, yielding a vanishing isocurvature fraction at N_{end} within numerical precision. The strong anti-correlation at crossing acts as a destructive interference mechanism that suppresses the adiabatic power at specific scales, imprinting a feature in the primordial spectrum without leaving a relic isocurvature contribution at the end of inflation. The top-left panel of Fig. 5 illustrates the spectral evolution at the pivot scale for $\xi_h = 0.1$. The difference with respect to the $\xi_h = 10^{-4}$ case is striking: following horizon crossing, the curvature power spectrum continues to undergo significant evolution driven by the turning rate $\eta_\perp$ until it stabilizes at a constant value,

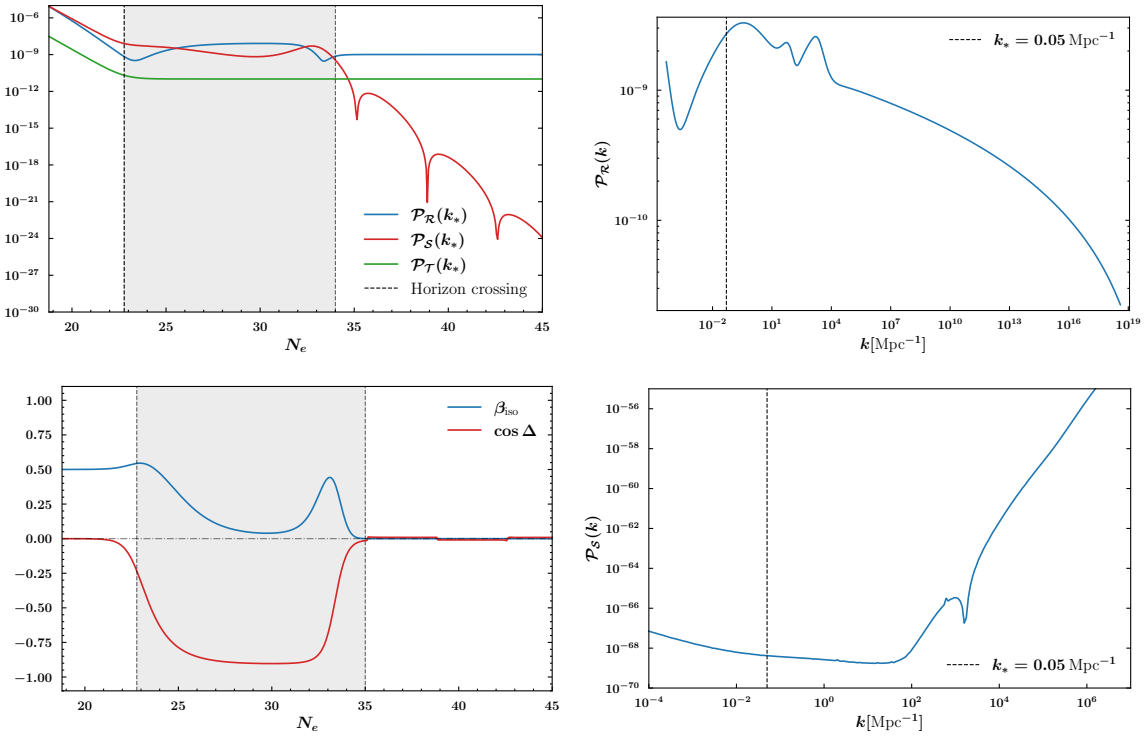

Figure 5. Primordial power spectra for curvature $\mathcal{P}_\mathcal{R}(k)$ (top), isocurvature $\mathcal{P}_\mathcal{S}(k)$ (middle), and the cross-correlation spectrum (bottom) for $\xi_h = 0.1$, $\lambda = 10^{-10}$ and $\xi_s = 4 \times 10^8$ evaluated at the end of inflation. The vertical dashed line corresponds to the scale pivot $k_* = 0.05\,\mathrm{Mpc}^{-1}$

marking its freeze-out. Conversely, the isocurvature spectrum is exponentially suppressed, reflecting its large effective mass and reducing its late-time impact on $\mathcal{R}_k$. This dynamics ensures that the isocurvature fraction $\beta_{\rm iso}$ becomes negligible at the end of inflation. The tensor spectrum remains practically unaltered in both scenarios, as expected. The top-right panel displays the resulting curvature power spectrum. Distinct oscillatory features arise naturally at scales $k \lesssim 10^4\,\mathrm{Mpc}^{-1}$, corresponding to the transition phase where the turning rate is significant and the slow-roll parameter exhibits a transient bump. At smaller scales, the spectrum recovers the scale-invariant prediction typical of single-field inflation driven by the scalaron (R^2) or the Higgs field h. The notable difference in this regime is that the amplitude of the adiabatic mode has been shifted due to the energy transfer from the isocurvature mode during the turn in field space. The bottom-left panel reveal a transient phase of coupling induced by the turning rate $\eta_\perp$ around $N_e \simeq 25 - 30$. This interaction generates a significant cross-correlation, reaching values of $\cos\Delta \approx -0.786$ at $k_* = 0.05\,\mathrm{Mpc}^{-1}$, and facilitates power transfer to the curvature spectrum, which is responsible for generating the features. Subsequently, due to the large effective mass of the Q_s field, isocurvature perturbations decay exponentially, and the modes decouple completely before the end of inflation. This results in purely adiabatic final observables, i.e., $\beta_{\rm iso} \to 0$, as shown in the bottom-right panel. Lastly, in the bottom-right panel we display the isocurvature power spectrum at the end of inflation. One can see that the isocurvature does not survive at the end of inflation, which is agreement with the isocurvature fraction $\beta_{\rm iso}$. For completeness, we performed a numerical scan over the non-minimal coupling in the range $\xi_h \in [0.08, 0.2]$.

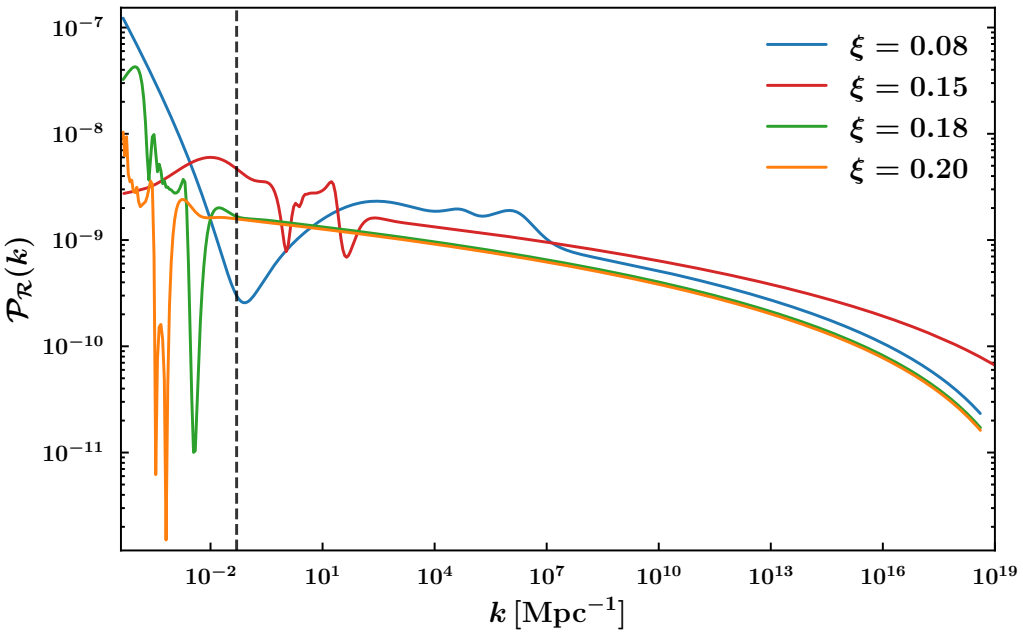

Figure 6. Adiabatic primordial power spectrum $\mathcal{P}_{\mathcal{R}}(k)$ evaluated at the end of inflation for λ and ξ_s fixed, and ξ_h is varied over four values. The vertical dashed line corresponds to the scale pivot $k_* = 0.05\,\mathrm{Mpc}^{-1}$.

As illustrated in Fig. 6, the position and depth of the spectral features are highly sensitive to ξ_h. We find that values outside the narrow window $\xi_h \approx 0.1 \pm 0.01$ shift the suppression scale away from the scales associated with the CMB low-ℓ suppression or wash out the features entirely. This suggests that if the low-ℓ deficit is of primordial origin, it points to a very specific tuning of the non-minimal coupling within the Higgs-R^2 model.

5 Impact on CMB observables

To confront the predictions of the multi-field Higgs-R^2 model with observational data, we compute the angular power spectra for temperature and polarization anisotropies. We process the primordial power spectra $P_{\mathcal{R}}(k)$ obtained in the previous section using the Boltzmann code `CLASS` [71], assuming a standard ΛCDM background cosmology consistent with the Planck 2018 best-fit parameters [5]. The power spectra (4.2) can be used to define th standard inflationary observables relevant to the CMB scales. Besides the isocurvature fraction (4.3) and the cross-correlation fraction (4.4), we also define the tensor to scalar ratio as the ratio between the amplitude of tensor and scalar perturbations, where scalar perturbations include adiabatic and isocurvature modes

$$r = \frac{\mathcal{P}_{\mathcal{T}}(k_*)}{\mathcal{P}_{\mathcal{R}}(k_*) + \mathcal{P}_{\mathcal{S}}(k_*)} \tag{5.1}$$

which is evaluated at the pivot scale $k_* = 0.05\mathrm{Mpc}^{-1}$. This expression can be rewritten in terms of the cross-correlation fraction as [6, 7, 9, 25, 26]

Non-minimal coupling	$N_{\rm hc}$	$P_{\mathcal{R}}(k_*)$	n_s	r	$\beta_{\rm iso}$	$\cos\Delta$
$\xi_h = 10^{-9}$	50	2.404×10^{-9}	0.9614	4.264×10^{-3}	0.0101	0
$\xi_h = 0.1$	50	2.083×10^{-9}	0.9687	4.925×10^{-3}	0	-0.7816

Table 1. CMB observables for Higgs-R^2 inflation with $\lambda = 10^{-10}$ $\xi_s = 4 \times 10^8$ fixed and the cases $\xi_h = 10^{-9}$ and $\xi_h = 0.1$ for non-minimal Higgs constant copuling. All observables were evaluated at the pivot scale $k_* = 0.05\,\mathrm{Mpc}^{-1}$

$$r = -n_{\mathcal{T}} \left(1 - \frac{\mathcal{C}_{\mathcal{RS}}}{\mathcal{P}_{\mathcal{R}}\mathcal{P}_{\mathcal{S}}}\right) = -8 n_{\mathcal{T}} \sin^2\Delta\,, \tag{5.2}$$

where $n_{\mathcal{T}}$ is the tensor spectral index, define as

$$n_{\mathcal{T}} = \frac{\mathrm{d}\log\mathcal{P}_{\mathcal{T}}}{\mathrm{d}\log k}\,, \tag{5.3}$$

and the scalar spectral index n_s is defined in the usual way

$$n_s - 1 = \frac{\mathrm{d}\log\mathcal{P}_{\mathcal{R}}}{\mathrm{d}\log k}\,. \tag{5.4}$$

The consistency relation (5.2) indicates that the amplitude of primordial gravitational waves is suppressed in multi-field inflation compared to the single-field expectation. Current observational constraints from the combination of Planck, BICEP/Keck, and BAO data place an upper limit on the tensor-to-scalar ratio of $r < 0.036$ at 95% CL [5, 72], while the updated value reported by ACT + Planck + SPT + DESI for the scalar spectral index is $n_s \approx 0.9728 \pm 0.0027$ [73]. The CMB observables are summarized in Table 1. As one can see, the model predicts a tensor to scalar ratio $r \sim \mathcal{O}(10^{-3})$, which satisfies this bound comfortably.

5.1 Connection to the low-ℓ anomaly

The anomaly in the large-scale power of the CMB temperature anisotropies, particularly the deficit in the quadrupole and octupole moments observed by Planck [5], challenges the standard ΛCDM paradigm. While usually attributed to cosmic variance, a physical origin remains a compelling possibility. In the literature, there have been various attempts to describe this power deficit, utilizing multi-field models with non-canonical kinetic terms [25], modifications to the inflationary epoch such as a brief kinetic regime imposing a cutoff on the primordial power spectrum [48], late-time effects like destructive interference caused by the integrated Sachs-Wolfe effect, or by introducing a class of potentials similar to those arising in minimal supersymmetric extensions of the Standard Model [49].

In the Higgs-R^2 model, the turning rate in field space generates localized features in the primordial power spectrum that naturally map onto the largest angular scales of the CMB last scattering surface, specifically at $\ell \lesssim 30$. In Figure 7, we present the lensed temperature auto-correlation spectrum, $\mathcal{D}_\ell^{TT} = \ell(\ell+1)C_\ell^{TT}/2\pi$, for our benchmark model with $\xi_h = 0.1$. To verify that this feature is unique to the non-minimal coupling dynamics, we compare it with the case $\xi_h = 10^{-9}$.

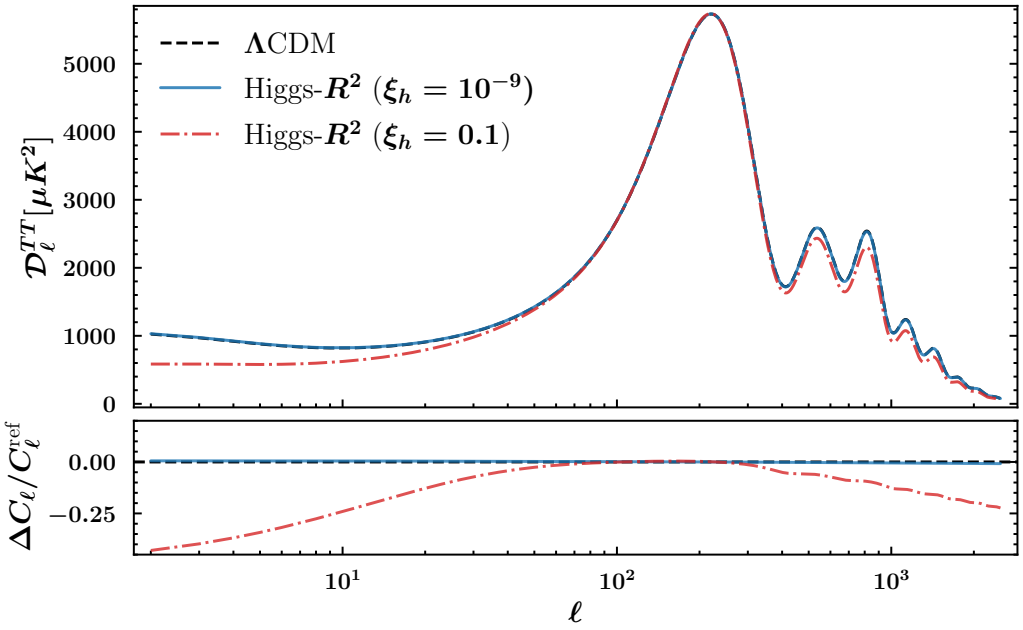

Figure 7. Comparison of the TT angular power spectrum for two representative choices of the Higgs non-minimal coupling ξ_h. For $\xi_h = 10^{-9}$ the model is observationally indistinguishable from ΛCDM, whereas $\xi_h = 0.1$ produces a characteristic suppression at low multipoles, with a residual about $\sim 25 - 30\%$, with accordance to Planck [5].

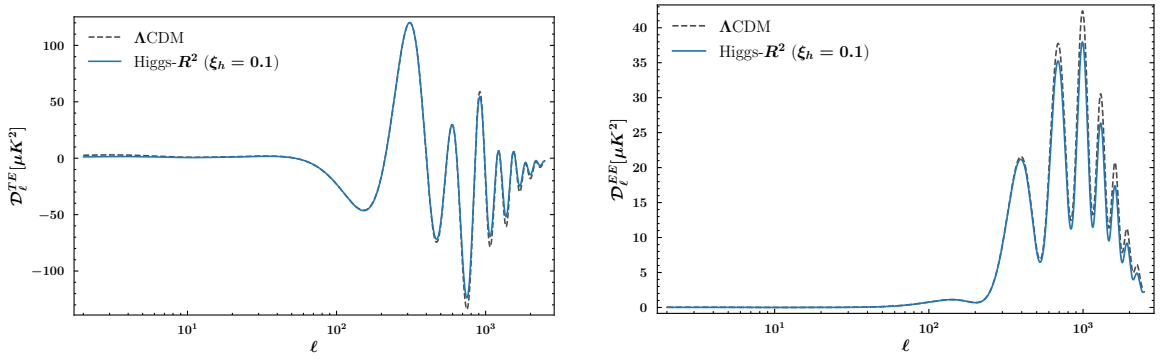

Figure 8. Angular power spectra for the TE cross-correlation (left panel) and EE polarization (right panel). The solid blue line represents the Higgs-R^2 model prediction for $\xi_h = 0.1$, while the dashed black line shows the ΛCDM baseline using Planck 2018 best-fit parameters.

As expected, the limit $\xi_h \ll 1$ limit provides a clean control case in which the model smoothly reduces to standard single-field dynamics, yielding angular spectra indistinguishable from ΛCDM. For the case $\xi_h = 0.1$, the theoretical prediction closely follows the data, exhibiting a suppression of approximately $25\% - 30\%$ at low-ℓ multipoles. As highlighted in the inset of Fig. 7, the residuals show a clear deviation from ΛCDM at $\ell \lesssim 30$, reducing the tension. Crucially, at smaller scales ($\ell \gtrsim 100$), the acoustic peaks are reproduced with high accuracy. The turning rate mechanism discussed in previous sections naturally produce features consistent with low-ℓ anomaly observed by Planck. The model preserves the stan-

dard acoustic phase and amplitude, ensuring consistency with the precise measurements of the damping tail. We further validate the physical consistency of the model by examining the polarization spectra. Figure 8 displays the cross-correlation (TE) and E-mode polarization (EE) spectra. The TE spectrum shows excellent agreement with the standard model, accurately reproducing the phase of the acoustic oscillations. This confirms that the turning dynamics, while suppressing power at large scales, preserve the adiabatic structure of the perturbations required by the data. A slight reduction in the amplitude of the EE acoustic peaks is observed when compared with the ΛCDM baseline. This effect is expected, as the EE spectrum is more sensitive to small variations in the amplitude and scale dependence of the primordial scalar spectrum, especially around intermediate scales. Given the significantly larger observational uncertainties in polarization compared to temperature, the predicted EE spectrum remains fully consistent with current constraints.

6 Discussion and conclusions

In this work, we have presented a comprehensive analysis of primordial perturbations in multi-field Higgs-R^2 inflation. By going beyond the effective single-field approximation and performing a full numerical integration of the background and perturbation equations, we have revealed a rich phenomenology controlled by the non-minimal coupling ξ_h. Our results demonstrate that the field-space geometry and the trajectory's turning rate play a decisive role in shaping the inflationary observables, leading to distinct signatures that are absent in the standard single-field limit. We identified two dynamical regimes depending on the magnitude of the Higgs non-minimal coupling. For weak coupling ($\xi_h \ll 1$), the turning rate $\eta_\perp$ is negligible, and the adiabatic power spectrum remains featureless. However, contrary to the standard heavy-field intuition, we found that the isocurvature mode Q_s remains light ($m_{\rm iso}^2 \lesssim H^2$) and fails to decay, leaving a residual isocurvature fraction $\beta_{\rm iso} \sim \mathcal{O}(10^{-2})$ at the end of inflation. This implies that in the weak coupling limit, Higgs-R^2 inflation is not effectively single-field, but rather a multi-field scenario with surviving isocurvature modes that could be constrained by future high-precision data.

The second, and perhaps most intriguing regime, appears for $\xi_h \sim 0.1$. In this case, the turning rate becomes significant as the trajectory transitions from the ridge at $h = 0$ towards the valley. This transient turn induces a strong coupling between adiabatic and isocurvature modes. We showed that this interaction results in a localized dip in the primordial curvature spectrum at large scales, followed by oscillatory features. Importantly, in this regime, the isocurvature modes eventually become heavy and decay exponentially, yielding a purely adiabatic spectrum at the end of inflation. When confronting these predictions with observations, we found that the spectral feature generated in the $\xi_h \sim 0.1$ scenario naturally maps onto the large angular scales of the CMB. This mechanism provides a physical explanation for the suppression of the low-ℓ multipoles observed by Planck, a feature that remains anomalous within the standard ΛCDM concordance model. Our analysis confirms that this suppression can be achieved without disrupting the acoustic peaks at smaller scales, maintaining consistency with the precise measurements of the CMB damping tail. Although our results indicate that the model can account for the low–ℓ CMB suppression, confirming this interpretation requires a dedicated likelihood evaluation. Given the large cosmic variance at $\ell \lesssim 30$, a full statistical comparison with the Planck low–ℓ likelihood is needed to determine whether the improvement over ΛCDM is significant. We leave this analysis for future work.

Given that the suppression of power in our model originates from transient multifield effects associated with a non-trivial turn in field space, it would be natural to investigate whether the same dynamics could leave signatures in higher-order correlation functions. In particular, the interplay between adiabatic-isocurvature mixing and the turn-rate suggests that this setup may lead to distinctive non-Gaussian features. We leave a quantitative analysis of primordial bispectra and constraints on $f_{\rm NL}$ for future work.

7 Acknowledgments

This work was partially supported by SECIHTI CBF2023-2024-1937 and FP has received the funding 803062 from SECIHTI-México.

A Single-field inflation along the valleys

The valley approximation of the potential (2.6) in the Einstein frame is relevant for analyzing the evolution of the fields (ϕ, h). This analysis has been discussed in detail in previous works on this model [31–33]; therefore, here we restrict ourselves to outlining the main ideas. In the limit $h \gg v_{\rm ew}$, the valleys of the potential (2.6) are defined by the condition

$$\frac{\partial V}{\partial h} = 0\,, \quad h_0^2(\phi) = \frac{\xi_h}{\xi_h^2 + 4\lambda\xi_s}(e^{\alpha\phi} - 1) \tag{A.1}$$

This condition represents a stationary point in the $(h, \dot{h})$ plane; as the scalaron ϕ rolls down to the minimum of the potential (2.6), the valleys act as a universal attractor. Since the potential is symmetric under $h \to -h$, Eq. (A.1) identifies the two valleys of $V(\phi, h)$. Along one of the valleys, the potential is given by the following effective potential as a function of ϕ:

$$V_{\rm eff}(\phi\,, h_0(\phi)) = \frac{\lambda}{4(\xi_h^2 + 4\lambda\xi_s)}(1 - e^{-\alpha\phi})^2\,. \tag{A.2}$$

This potential has exactly the same form as the potential in R^2 inflation or the Higgs inflation model [34]. For the standard parameter space discussed above, the model effectively reduces to a single scalar field model. Given that the Higgs field along the valleys is determined by (A.1), the action (2.4) along these trajectories takes the form

$$S_E[g_\mu\,, \phi\,, h] = \int \mathrm{d}^4x\,\sqrt{-g}\,\left[\frac{1}{2}R - \frac{1}{2}g^{\mu\nu}\partial_\mu\phi\partial_\nu\phi\left(1 + \gamma^2(1 - e^{-\alpha\phi})^{-1}\right) - V_{\rm eff}(\phi)\right]\,, \tag{A.3}$$

where $\tilde{\xi}^2 = \frac{\xi_h}{6(\xi_h^2 + 4\lambda\xi_s)}$. We observe that if $\lambda = 0.13$ and $\xi_h \sim 10^4$, the constant is of the order $\tilde{\xi} \sim 10^{-5}$; thus, the second factor in the kinetic term becomes subdominant. At the inflationary scale $\phi \gg 1$, the model effectively reduces to canonical single-field inflation with the effective potential given by (A.2). However, for a parameter space such that $\xi_h \sim \lambda\xi_s$, the constant becomes $\tilde{\xi} \sim \mathcal{O}(1)$. This case corresponds to what is known as the quasi-single field inflation regime [16, 70]. Along the valleys, both the unit vectors and the turning rate adopt a simplified form:

$$T^I = \frac{(1\,,\tilde{\xi}e^{\alpha\phi/2})}{\sqrt{1+\tilde{\xi}^2}}\,, \quad N^I = \frac{(-\tilde{\xi}\,,e^{\alpha\phi/2})}{\sqrt{1+\tilde{\xi}^2}}\,, \quad \eta_\perp = \frac{\tilde{\xi}}{\sqrt{1+\tilde{\xi}^2}} \tag{A.4}$$

If $\tilde{\xi} \ll 1$, the vector T^I aligns with the ϕ direction, while N^I points in the h direction. The turning rate $\eta_\perp$ is negligible within the valleys.

References

[1] A. H. Guth, *Inflationary universe: A possible solution to the horizon and flatness problems*, *Phys. Rev. D* **23** (1981) 347.

[2] A. Linde, *A new inflationary universe scenario: A possible solution of the horizon, flatness, homogeneity, isotropy and primordial monopole problems*, *Physics Letters B* **108** (1982) 389.

[3] A. R. Liddle and S. M. Leach, *How long before the end of inflation were observable perturbations produced?*, *Phys. Rev. D* **68** (2003) 103503.

[4] E. D. Stewart and D. H. Lyth, *A more accurate analytic calculation of the spectrum of cosmological perturbations produced during inflation*, *Physics Letters B* **302** (1993) 171.

[5] Y. Akrami, F. Arroja, M. Ashdown, J. Aumont, C. Baccigalupi, M. Ballardini et al., *Planck 2018 results-x. constraints on inflation*, *Astronomy & Astrophysics* **641** (2020) A10.

[6] D. Wands, N. Bartolo, S. Matarrese and A. Riotto, *Observational test of two-field inflation*, *Phys. Rev. D* **66** (2002) 043520.

[7] N. Bartolo, S. Matarrese and A. Riotto, *Adiabatic and isocurvature perturbations from inflation: Power spectra and consistency relations*, *Phys. Rev. D* **64** (2001) 123504.

[8] I. Huston and A. J. Christopherson, *Calculating nonadiabatic pressure perturbations during multifield inflation*, *Phys. Rev. D* **85** (2012) 063507.

[9] F. Di Marco, F. Finelli and R. Brandenberger, *Adiabatic and isocurvature perturbations for multifield generalized einstein models*, *Phys. Rev. D* **67** (2003) 063512.

[10] V. Mukhanov and P. J. Steinhardt, *Density perturbations in multifield inflationary models*, *Physics Letters B* **422** (1998) 52.

[11] Z. Lalak, D. Langlois, S. Pokorski and K. Turzyński, *Curvature and isocurvature perturbations in two-field inflation*, *Journal of Cosmology and Astroparticle Physics* **2007** (2007) 014.

[12] A. A. Starobinsky, S. Tsujikawa and J. Yokoyama, *Cosmological perturbations from multi-field inflation in generalized einstein theories*, *Nuclear Physics B* **610** (2001) 383.

[13] D. Langlois, *Correlated adiabatic and isocurvature perturbations from double inflation*, *Phys. Rev. D* **59** (1999) 123512.

[14] D. Langlois, *Isocurvature cosmological perturbations and the cmb*, *Comptes Rendus Physique* **4** (2003) 953.

[15] S. Garcia-Saenz, L. Pinol and S. Renaux-Petel, *Revisiting non-gaussianity in multifield inflation with curved field space*, *Journal of High Energy Physics* **2020** (2020) .

[16] X. Chen and Y. Wang, *Quasi-single field inflation and non-gaussianities*, *Journal of Cosmology and Astroparticle Physics* **2010** (2010) 027–027.

[17] T. Battefeld and R. Easther, *Non-gaussianities in multi-field inflation*, *Journal of Cosmology and Astroparticle Physics* **2007** (2007) 020–020.

[18] F. Bernardeau and J.-P. Uzan, *Non-gaussianity in multifield inflation*, *Physical Review D* **66** (2002) .

[19] O. Iarygina, M. D. Marsh and G. Salinas, *Non-gaussianity in rapid-turn multi-field inflation*, *Journal of Cosmology and Astroparticle Physics* **2024** (2024) 014.

[20] D. I. Kaiser, E. A. Mazenc and E. I. Sfakianakis, *Primordial bispectrum from multifield inflation with nonminimal couplings*, *Phys. Rev. D* **87** (2013) 064004.

[21] J. Elliston, D. Seery and R. Tavakol, *The inflationary bispectrum with curved field-space*, *Journal of Cosmology and Astroparticle Physics* **2012** (2012) 060–060.

[22] K. Schutz, E. I. Sfakianakis and D. I. Kaiser, *Multifield inflation after planck: Isocurvature modes from nonminimal couplings*, *Phys. Rev. D* **89** (2014) 064044.

[23] D. I. Kaiser and E. I. Sfakianakis, *Multifield inflation after planck: The case for nonminimal couplings*, *Physical Review Letters* **112** (2014) .

[24] D. I. Kaiser and A. T. Todhunter, *Primordial perturbations from multifield inflation with nonminimal couplings*, *Phys. Rev. D* **81** (2010) 124037.

[25] M. Braglia, D. K. Hazra, F. Finelli, G. F. Smoot, L. Sriramkumar and A. A. Starobinsky, *Generating pbhs and small-scale gws in two-field models of inflation*, *Journal of Cosmology and Astroparticle Physics* **2020** (2020) 001–001.

[26] F. Di Marco and F. Finelli, *Slow-roll inflation for generalized two-field lagrangians*, *Physical Review D* **71** (2005) .

[27] A. Achúcarro, J.-O. Gong, S. Hardeman, G. A. Palma and S. P. Patil, *Features of heavy physics in the cmb power spectrum*, *Journal of Cosmology and Astroparticle Physics* **2011** (2011) 030.

[28] S. Céspedes, V. Atal and G. A. Palma, *On the importance of heavy fields during inflation*, *Journal of Cosmology and Astroparticle Physics* **2012** (2012) 008.

[29] X. Gao, D. Langlois and S. Mizuno, *Influence of heavy modes on perturbations in multiple field inflation*, *Journal of Cosmology and Astroparticle Physics* **2012** (2012) 040–040.

[30] Y. Ema, *Higgs scalaron mixed inflation*, *Physics Letters B* **770** (2017) 403.

[31] M. He, A. A. Starobinsky and J. Yokoyama, *Inflation in the mixed higgs-r2 model*, *Journal of Cosmology and Astroparticle Physics* **2018** (2018) 064–064.

[32] Y.-C. Wang and T. Wang, *Primordial perturbations generated by higgs field and R^2 operator*, *Phys. Rev. D* **96** (2017) 123506.

[33] A. Gundhi and C. F. Steinwachs, *Scalaron-higgs inflation*, *Nuclear Physics B* **954** (2020) 114989.

[34] F. Bezrukov and M. Shaposhnikov, *The standard model higgs boson as the inflaton*, *Physics Letters B* **659** (2008) 703.

[35] A. Salvio and A. Mazumdar, *Classical and quantum initial conditions for higgs inflation*, *Physics Letters B* **750** (2015) 194.

[36] D. Gorbunov and A. Tokareva, *Scalaron the healer: removing the strong-coupling in the higgs- and higgs-dilaton inflations*, *Physics Letters B* **788** (2019) 37.

[37] F. Bezrukov, D. Gorbunov, C. Shepherd and A. Tokareva, *Some like it hot: R2 heals higgs inflation, but does not cool it*, *Physics Letters B* **795** (2019) 657.

[38] M. He, *Perturbative reheating in the mixed Higgs-R2model*, *Journal of Cosmology and Astroparticle Physics* **2021** (2021) [2010.11717].

[39] M. He, R. Jinno, K. Kamada, S. C. Park, A. A. Starobinsky and J. Yokoyama, *On the violent preheating in the mixed Higgs-R 2 inflationary model*, *Physics Letters, Section B: Nuclear, Elementary Particle and High-Energy Physics* **791** (2019) 36 [1812.10099].

[40] M. He, R. Jinno, K. Kamada, A. A. Starobinsky and J. Yokoyama, *Occurrence of tachyonic preheating in the mixed Higgs-R2 model*, *Journal of Cosmology and Astroparticle Physics* **2021** (2021) 20 [2007.10369].

[41] F. Pineda and L. O. Pimentel, *Non-perturbative approach for scalar particle production in higgs-r^2 inflation*, *The European Physical Journal C* **85** (2025) 731.

[42] R. Durrer, O. Sobol and S. Vilchinskii, *Magnetogenesis in higgs-starobinsky inflation*, *Physical Review D* **106** (2022) .

[43] Y. Ema and S. Verner, *Cosmological collider signatures of higgs-r2 inflation*, *Journal of Cosmology and Astroparticle Physics* **2024** (2024) 039.

[44] J. Kim, Z. Yang and Y.-l. Zhang, *Gravitational wave signatures of preheating in Higgs-R2 inflation*, *Phys. Rev. D* **112** (2025) 043534 [2503.16907].

[45] D. Y. Cheong, S. M. Lee and S. C. Park, *Primordial black holes in higgs-r2 inflation as the whole of dark matter*, *Journal of Cosmology and Astroparticle Physics* **2021** (2021) 032.

[46] D. Y. Cheong, K. Kohri and S. C. Park, *The inflaton that could: primordial black holes and second order gravitational waves from tachyonic instability induced in higgs-r2 inflation*, *Journal of Cosmology and Astroparticle Physics* **2022** (2022) 015.

[47] T. Modak, *R^2-higgs inflation: R^3 contribution and preheating after act and spt data*, *Phys. Rev. D* **112** (2025) 115006.

[48] C. R. Contaldi, M. Peloso, L. Kofman and A. Linde, *Suppressing the lower multipoles in the cmb anisotropies*, *Journal of Cosmology and Astroparticle Physics* **2003** (2003) 002–002.

[49] R. K. Jain, P. Chingangbam, J.-O. Gong, L. Sriramkumar and T. Souradeep, *Punctuated inflation and the low cmb multipoles*, *Journal of Cosmology and Astroparticle Physics* **2009** (2009) 009–009.

[50] J. Chluba, J. Hamann and S. P. Patil, *Features and new physical scales in primordial observables: Theory and observation*, *International Journal of Modern Physics D* **24** (2015) 1530023.

[51] J. L. F. Barbón and J. R. Espinosa, *On the naturalness of higgs inflation*, *Physical Review D* **79** (2009) .

[52] C. Burgess, H. M. Lee and M. Trott, *Power-counting and the validity of the classical approximation during inflation*, *Journal of High Energy Physics* **2009** (2009) 103–103.

[53] D. I. Kaiser, *Conformal transformations with multiple scalar fields*, *Physical Review D* **81** (2010) .

[54] A. J. Tolley and M. Wyman, *Equilateral non-gaussianity from multifield dynamics*, *Physical Review D* **81** (2010) .

[55] S. Cremonini, Z. Lalak and K. Turzyński, *Strongly coupled perturbations in two-field inflationary models*, *Journal of Cosmology and Astroparticle Physics* **2011** (2011) 016–016.

[56] J.-O. Gong and T. Tanaka, *A covariant approach to general field space metric in multi-field inflation*, *Journal of Cosmology and Astroparticle Physics* **2011** (2011) 015.

[57] J.-O. Gong, *Multi-field inflation and cosmological perturbations*, *International Journal of Modern Physics D* **26** (2017) 1740003 [https://doi.org/10.1142/S021827181740003X].

[58] S. Karamitsos and A. Pilaftsis, *Frame covariant nonminimal multifield inflation*, *Nuclear Physics B* **927** (2018) 219.

[59] J. Fumagalli, S. Renaux-Petel and L. T. Witkowski, *Oscillations in the stochastic gravitational wave background from sharp features and particle production during inflation*, *Journal of Cosmology and Astroparticle Physics* **2021** (2021) 030.

[60] S. S. Mishra and V. Sahni, *Primordial black holes from a tiny bump/dip in the inflaton potential*, *Journal of Cosmology and Astroparticle Physics* **2020** (2020) 007–007.

[61] R. Arnowitt, S. Deser and C. W. Misner, *Republication of: The dynamics of general relativity*, *General Relativity and Gravitation* **40** (2008) 1997–2027.

[62] J. Maldacena, *Non-gaussian features of primordial fluctuations in single field inflationary models*, *Journal of High Energy Physics* **2003** (2003) 013–013.

[63] D. Langlois and S. Renaux-Petel, *Perturbations in generalized multi-field inflation*, *Journal of Cosmology and Astroparticle Physics* **2008** (2008) 017.

[64] M. Sasaki and E. D. Stewart, *A General Analytic Formula for the Spectral Index of the Density Perturbations Produced during Inflation*, *Progress of Theoretical Physics* **95** (1996) 71 [https://academic.oup.com/ptp/article-pdf/95/1/71/5377016/95-1-71.pdf].

[65] C. Gordon, D. Wands, B. A. Bassett and R. Maartens, *Adiabatic and entropy perturbations from inflation*, *Phys. Rev. D* **63** (2000) 023506.

[66] D. Seery and J. E. Lidsey, *Primordial non-gaussianities in single-field inflation*, *Journal of Cosmology and Astroparticle Physics* **2005** (2005) 003–003.

[67] D. H. Lyth, K. A. Malik and M. Sasaki, *A general proof of the conservation of the curvature perturbation*, *Journal of Cosmology and Astroparticle Physics* **2005** (2005) 004.

[68] D. H. Lyth and Y. Rodríguez, *Non-gaussianity from the second-order cosmological perturbation*, *Physical Review D* **71** (2005) .

[69] V. Mukhanov, H. Feldman and R. Brandenberger, *Theory of cosmological perturbations*, *Physics Reports* **215** (1992) 203.

[70] X. Chen and Y. Wang, *Large non-gaussianities with intermediate shapes from quasi-single-field inflation*, *Phys. Rev. D* **81** (2010) 063511.

[71] J. Lesgourgues, *The Cosmic Linear Anisotropy Solving System (CLASS) I: Overview*, 1104.2932.

[72] P. Ade, Z. Ahmed, M. Amiri, D. Barkats, R. B. Thakur, C. Bischoff et al., *Improved constraints on primordial gravitational waves using planck , wmap, and bicep/ keck observations through the 2018 observing season*, *Physical Review Letters* **127** (2021) .

[73] E. Calabrese, J. C. Hill, H. T. Jense, A. La Posta, I. Abril-Cabezas, G. E. Addison et al., *The atacama cosmology telescope: Dr6 constraints on extended cosmological models*, *Journal of Cosmology and Astroparticle Physics* **2025** (2025) 063.